Organic & Biomolecular Chemistry

Accepted Manuscript

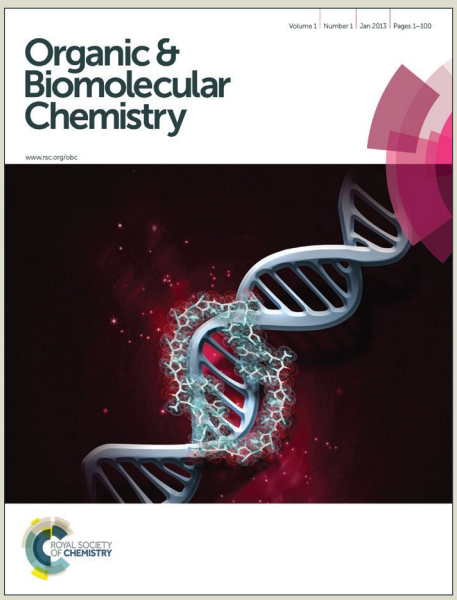

ROYAL SOCIETY OF CHEMISTRY

www.rsc.org/obc

Journal Name

ARTICLE

Evaluating hydrogen bonding control in the diastereoselective Diels-Alder reactions of 9-(2-aminoethyl)-anthracene derivatives

Received 00th January 20xx,
Accepted 00th January 20xx

DOI: 10.1039/x0xx00000x

www.rsc.org/

R. A. Bawa,[a] F.-M. Gautier,[a] H. Adams,[a] A. J. H. M. Meijer[a,*] and S. Jones[a,*]

Several 9-(2-aminoethyl)anthracene derivatives were prepared with different nitrogen substitutents including alkyl, acetamide, trifluoroacaeamide and t-butyl carbamate. The selectivity in Diels_alder cyclodaddition reaction with *N*-methyl maleimide was evaluated thorugh single crystal x-ray analysis of the products. Models for the change in selectivity with hydrogen bond acceptor are proposed, supported by DFT level calculations.

Introduction

Hydrogen bonding has been known to play a pivotal role in helping to control the stereochemical outcome of many chemical transformations, including the Diels-Alder reaction. In this respect, a number of seminal studies have investigated the nature of this control,[1–3] applied it in the design of catalysts,[4,5] and used it to access complex target molecules.[6] Previous work described from these laboratories[7–11] and others[12–17] on the cycloaddition of dienophiles to chiral anthracenes (eg **1**, **2**) has demonstrated an inherent preference of the stereodirecting group to deliver a single diastereoisomer of cycloadduct. This is caused by the subtle interplay of a number of interactions in the transition state connecting reactants and products, including a hydrogen bond, initiated by the group at the 9-position of the anthracene **1a** / **1b**, framed against a hydrogen bond from a C-H bond of the incoming dienophile with a lone pair on an electronegative element on the 9-position. A similar effect was also observed in 9-amino anthracene derivatives **2a** whereby this balance could be disrupted by methylation of the nitrogen atom **2b**, removing the hydrogen bond (Figure 1).[18,19,20,21,22,23]

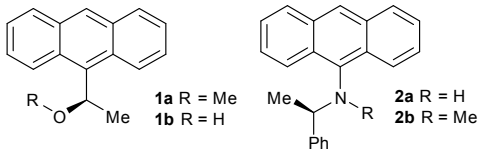

Figure 1 Anthracene derivative previously investigated

Thus, changing the relative position and strength of the hydrogen-bond donor and acceptor should change the diastereoselectivity. This effect can straight forwardly be achieved by replacing the oxygen atom in **1a** and **1b** with nitrogen, that would then allow control of the availability of the lone-pair on the nitrogen atom (i.e. the hydrogen-bond acceptor) in going from a secondary amine to an amide. The strength of the hydrogen-bond donor (the N-H) can be then be further attenuated by changing that nature of the amide group. It should be noted that in the case of a secondary amine, such as benzyl amine, there will be a number of additional possible H-bond donors (C-H) groups on the stereodirecting group to consider. The synthesis and reactions of these systems are described herein, supported with DFT calculations that attempt to elucidate the relative importance of H-bond donor and H-bond acceptor in these processes.

Results and discussion

Synthesis of the key α-methyl-9-anthracenemethanamine **3** was first attempted, which could then serve as a common intermediate for several of the diene substrates (Scheme 1).

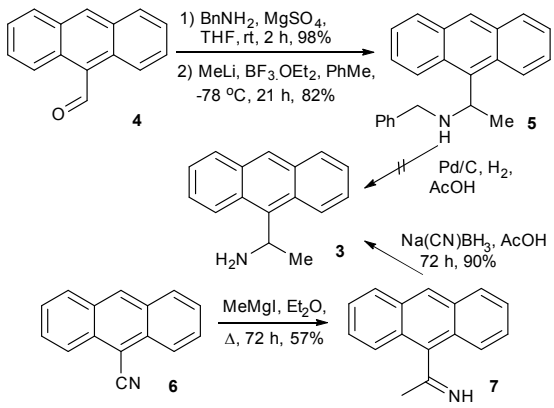

Scheme 1 Synthesis of α-methyl-9-anthracenemethanamine **1**

[a] *Department of Chemistry, University of Sheffield, Dainton Building, Brook Hill, Sheffield, S3 7HF. UK.*

† Electronic Supplementary Information (ESI) available Electronic supplementary information (ESI) available: copies of ^{1}H and ^{13}C NMR spectra, X-ray crystallographic details. CCDC 1409974 (**11**), 1409977 (**12**), 1409975 (**13**), and 1409976 (**14**), and all data for the calculations.
See DOI: 10.1039/x0xx00000x

The condensation of 9-anthraldehyde **4** with benzylamine in the presence of $MgSO_4$, followed by a Lewis acid mediated addition of MeLi to the resultant imine afforded the amine **5** in an overall yield of 80%. However, attempts to remove the benzyl group under standard hydrogenation conditions failed. Therefore, an alternative route was targeted, where 9-anthracenecarbonitrile **6** was first converted to the imine **7** by addition of methylmagnesium iodide, and subsequent reduction with $Na(CN)BH_3$ furnished the desired amine **3** in 90% yield. With amine **1** in hand, functionalization of the amine was achieved by treatment with the appropriate anhydride to generate the amides **8** and **9**, and carbamate **10** (Scheme 2).

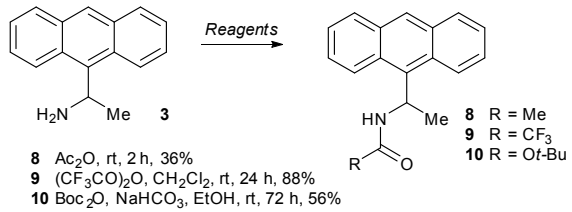

Scheme 2 Synthesis of amides **8** & **9** and carbamate **10**

Each of the amine derivatives was subsequently subjected to Diels-Alder reactions by heating at 80 °C in toluene with one equivalent of *N*-methyl maleimide. For comparison purposes, the methoxyethyl anthracene **1a** used extensively in previous work was also considered (Table 1).

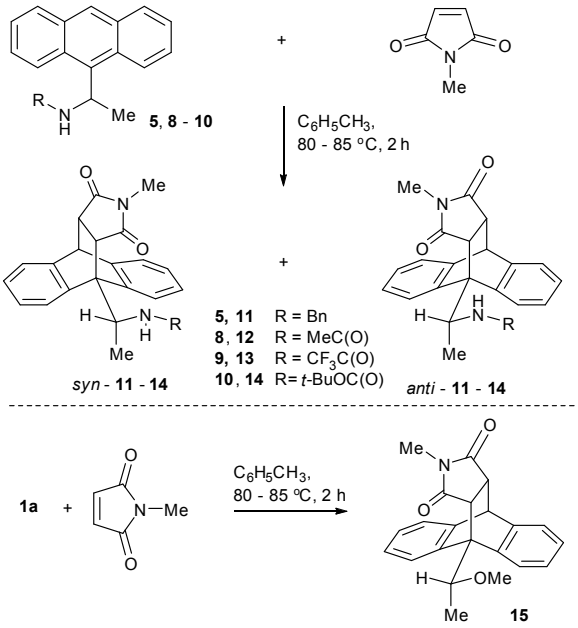

Scheme 3 Evaluation of anthracene derivatives in Diels-Alder reactions.

In all cases, the conversion and diastereoselectivity was calculated by comparison of the integrals in the ^{1}H NMR spectrum of the crude reaction mixture, and the identity of the major diastereoisomer confirmed by single crystal x-ray diffraction (see Figure 2 for a representative structure). It

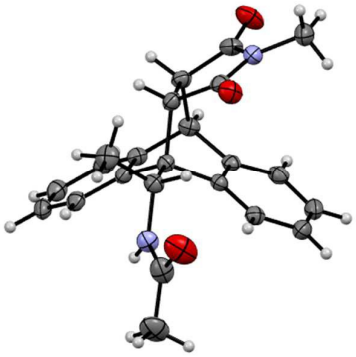

Figure 2 Representative X-ray crystal structure of cycloadduct **12**.

should be noted that in all structures obtained, steric influences from packing and / or intermolecular hydrogen bonds appear to override any preference to form intramolecular hydrogen bonds. The terms *anti* and *syn* used throughout refer to the relative orientation of the maleimide carbonyl group and the nitrogen atom attached to the 9-position of the anthracene, when the methyl group is placed perpendicular to the plane of the anthracene ring.

Table 1 Conversion and diastereomeric ratio from Diels-Alder reactions, as in Scheme 3

Entry	R	Conversion (%)[a]	Product	*anti*[b]	*syn*[b]
1	BnNH	84	**11**	72	18
2	MeC(O)NH	84	**12**	10	90
3	$CF_3C(O)NH$	100	**13**	25	75
4	*t*-BuOC(O)NH	78	**14**	20	80
5	MeO	100	**15**	100	0

[a] Determined from comparison of the integrals of the residual starting material and product(s) in the ^{1}H NMR spectrum of the crude reaction mixture. [b] Ratio determined by comparison of the integrals for the *syn* and *anti* isomers from in the ^{1}H NMR spectrum of the crude reaction mixture. The identity of the isomers was determined by single crystal x-ray diffraction.

In all cases, purification invariably led to samples of scalemic mixtures with diastereomeric ratios different to those obtained from the reaction. When such samples were subjected to the original reaction condition, no change in the diastereomeric ratio was observed, indicating that the reaction appears to proceed under kinetic control. The amine (Table 1, entry 1) gave the *anti* isomer as the major product, in-line with what would be expected by comparison with the ether **1a**. All other compounds (entries 2-4) show a reversal in the sense of diastereoselectivity.

To further substantiate this, the Gibbs energy for reaction, $\Delta_r G$, and the corresponding Gibbs energy of activation, $\Delta G^{\ddagger}$, were calculated by Density Functional Theory (DFT) methods for each of the substrates **5**, **8-10** (Table 2, for complete details, see experimental section). As in previous studies, the lowest energy conformation leading to each of the *syn* and *anti*-products that locates one of the groups attached to the 9-position orthogonal to the plane of ring was considered.

Table 2. Computational data for reaction outlined in Scheme 3.

		anti		*syn*[b]	
Anthracene	Approach[a]	$\Delta_r G^b$	$\Delta G^{‡,b}$	$\Delta_r G^b$	$\Delta G^{‡,b}$
5	α	1.7	**140.4**	23.5	**142.4**
	β	12.0	163.4	24.1	171.3
	γ	33.7	157.0	6.9	148.6
8	α	13.8	**148.3**	16.1	**138.3**
	β	-0.9	152.6	22.8	**138.3**[c]
	γ	24.1	153.0	0.6	145.3
9	α	9.6	**146.2**	14.9	**143.0**
	β	-4.7	153.9	23.6	165.2
	γ	23.3	153.1	-0.3	145.9
10	α	12.6	**147.1**	18.8	**142.7**
	β	-0.5	154.0	21.7	164.7
	γ	23.4	149.7	-1.0	145.5

[a] Orientation of group placed orthogonal to plane of anthracene ring; in 'α' Me is orthogonal, 'β' R is orthogonal and in 'γ' the H atom is orthogonal. [b] in kJ mol^{-1}. [c] Converts to approach *syn*-α during optimization.

Benzyl amine **5** bears the closest similarity to the ether **1a** which has been previously investigated, and contains a hydrogen-bond accepting electronegative nitrogen atom and a hydrogen-bond donor (CH) adjacent to this atom, as in the case of the ether **1a**. However, in contrast to the ether **1a**, the amine **5** can function as a hydrogen-bond donor as well, akin to the alcohol, **1b**. Comparing the different energies, $\Delta G^{‡}$, for the benzyl amine **8**, it is clear that it behaves more like ether **1a** than the alcohol **1b**. The relevant structures for the lowest transition state for *anti* and *syn* isomers clearly show that in the lowest energy transition state, the stereodirecting group is able to adopt a pincer-like conformation, where the nitrogen atom, acting as a hydrogen-bond acceptor and the hydrogen-bond donor are not connected to each other, leading to two possible cooperative conformations [Figure 3, panels (a) and (b)].

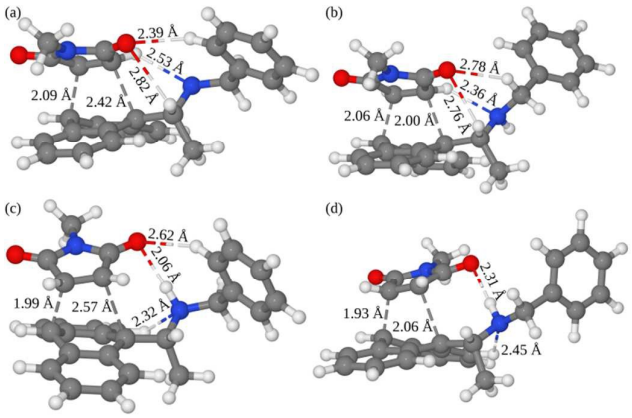

Figure 3 Different possible transition states for *N*-methyl maleimide with anthracene **5**. Panel (a): lowest TS for the *anti* approach (140.39 kJ mol^{-1}). Panel (b): Second-lowest TS for the *anti* approach (140.40 kJ mol^{-1}). Panel (c): Lowest TS for the *syn* approach (142.4 kJ mol^{-1}). Panel (d): Second-lowest TS for the *syn* approach (143.7 kJ mol^{-1}).

In panel (a), a CH from the phenyl ring serves as the H-bond donor, whereas in panel (b) it is a CH from the methylene bridge unit. This leads to a barrier height for panel (a) being 0.01 kJ mol^{-1} lower than for panel (b). It is also noticeable that in panel (b) the transition state is essentially synchronous, compared to the clearly asynchronous one in panel (a), showing that (a)synchronicity for this system is not a diagnostic for the barrier height.[21]

In the case of the lowest transition states for the *syn*-isomer [Figure 3, panels (c) and (d)] the conformation of the stereodirecting group has clearly changed compared to the *anti* to avoid clash of the methyl group with the incoming dienophile. As a consequence, the stereochemistry around the nitrogen atom is inverted, to facilitate NH interactions with the maleimide, thus eliminating any maleimide interactions with the lone pair of the nitrogen atom, which instead accepts a hydrogen bond from a C-H on the anthracene backbone. Another aromatic C-H interaction with the maleimide is also observed, as in panel (a). Finally, in panel (d), the benzyl unit rotates away, allowing the transition state to be more synchronous. However, the slightly longer NH···O bond means that this transition state is 1.31 kJ mol^{-1} higher in energy, but since this is less than the thermal energy of the reaction temperature, it will still have a role to play. These conclusions are consistent with the experimental results previously obtained for the ether **1a** and alcohol **1b**. In the case of the ether **1a**, the hydrogen-bond donor and acceptor components are not directly connected. As a consequence, the stereodirecting group has enough flexibility to form a pincer-like conformation and stabilize the transition state that leads to the *anti*-isomer as the major product. For the alcohol **1b**, the hydrogen-bond donor and acceptor are both associated with the hydroxyl group. As a consequence, only one of these two functionalities can be used to stabilize the transition state, which turns out to be the hydrogen-bond donating ability. Given this and the geometric constraints of the stereogenic centre, the major product will be *syn*.

Based on these arguments, a number of predictions for amide derivatives **8**-**10** can be made. Here, the conjugation of the nitrogen atom in the amide group can only lead to this functioning as a hydrogen-bond donor. In addition, the planar nature of this functional group means that the alkyl and alkoxy groups attached will be too far away to interact directly with the functional groups of the dienophile and may only influence the hydrogen-bond donating ability of the amide NH subgroup. Thus, one would expect these systems to behave as the alcohol **1b** and give the *syn*-isomer as the major product. The experimental (Table 1) and computational data (Table 2) confirm this. For example, the lowest transition state for trifluoroacetamide **9** clearly shows this predicted behaviour [Figure 4, panel (a)].

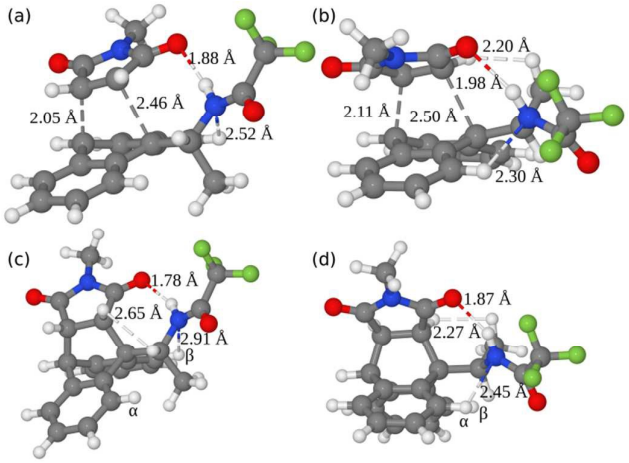

Figure 4. Transition state geometries and final geometries for two isomers of the $CF_3C(O)NH$ cycloaddition reaction. Panels (a) and (b) show the transition state for the *syn* conformation (α-approach, 143.0 kJ mol^{-1}), and *anti*-conformation (β-approach, 153.9 kJ mol^{-1}), respectively. Panel (c) and (d) show the corresponding final products *syn*-**13** (14.9 kJ mol^{-1}) and *anti* **13** (-4.7 kJ mol^{-1}).

This data also reaffirms earlier reported work that the lowest transition state does not necessarily correlate to the most stable product in these reactions, confirming the experimental observation that the reaction occurs under kinetic control. For example, if the two lowest energy transition states for the trifluoroacetamide **9** and associated products are compared (Figure 4), it is clear for the *syn* addition shown in panels (a) and (c) that the most important distances are very similar, whereby the distances for the *anti* conformation shown in panels (b) and (d) are consistently larger, making the transition state earlier, *i.e.* more reactant-like. This is probably caused by the fact that for the *anti*-approach, the methyl group clashes with a hydrogen atom on the incoming maleimide. For the *syn*-approach shown in panel (a) the distance between hydrogen atom at the stereogenic centre and the hydrogen atom on the maleimide is 2.9 Å, leading to a lower transition state energy. It should be noted that both cases are equally asynchronous, suggesting again that the synchronicity of the transition state is not necessarily a marker for the height of the transition state. In contrast the Gibbs energy of the final product for the *anti*-configuration is 19.6 kJ mol^{-1} lower. Again, this is not due to the amide, but rather that in the *anti*-approach [panel (b)] the two halves of the anthracene 'hinge' can come closer together, because the hydrogen atom on the stereogenic centre is pointing down, rather than the methyl group as in panel (a). This is reflected in the fact that in panel (c) the hydrogen atoms marked α and β are 4.93 Å apart, whereas in panel (d) the equivalent distance is 4.53 Å. Similar conclusions can be drawn for the MeC(O)NH and *t*-BuOC(O) substrates (see Figure 5 and 6, respectively).

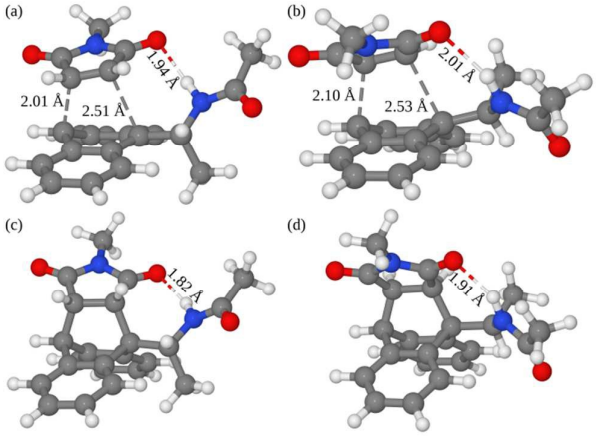

Figure 5. Transition state geometries and final geometries for two isomers of the MeC(O)NH cycloaddition reaction. Panels (a) and (b) show the transition state for the *syn* conformation (α-approach, 138.3 kJ mol^{-1}), and *anti*-conformation (β-approach, 152.6 kJ mol^{-1}), respectively. Panel (c) and (d) show the corresponding final products *syn*-**12** (16.1 kJ mol^{-1}) and *anti* **12** (-0.9 kJ mol^{-1}).

If it is assumed that the Eyring-Polyani equation holds, the relative rate of formation for the *syn* and *anti* isomers can be written as:

$$\frac{k_{anti}}{k_{syn}} = e^{-\Delta\Delta G^{\ddagger}}$$

where $\Delta\Delta G^{\ddagger}$ is defined as $\Delta G^{\ddagger}_{anti} - \Delta G^{\ddagger}_{syn}$. However, it needs to be noted that in the case of BnNH, in particular, one needs to take account of all thermally accessible transition states. Also, for completeness and comparison purposes, results from earlier work on the MeO derivative **1a** are included (Table 3).[18]

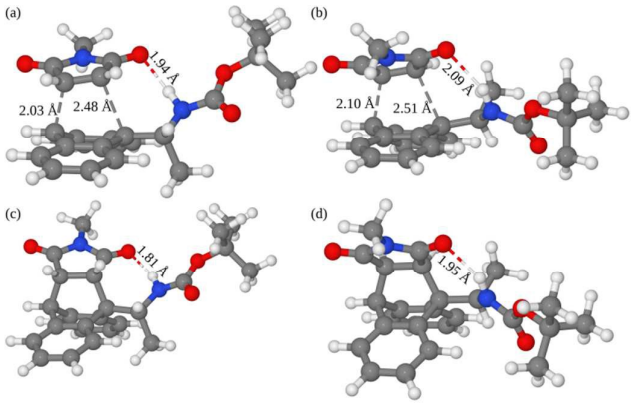

Figure 6. Transition state geometries and final geometries for two isomers of the *t*-BuO(O)NH cycloaddition reaction. Panels (a) and (b) show the transition state for the *syn* conformation (α-approach, 142.7 kJ mol^{-1}), and *anti*-conformation (β-approach, 154.0 kJ mol^{-1}), respectively. Panel (c) and (d) show the corresponding final products *syn*-**14** (18.8 kJ mol^{-1}) and *anti* **14** (-0.5 kJ mol^{-1}).

Table 3 Comparison of computed ratios for two different approaches with experimental results

		Lowest TS only	*All TSs*	*Experimental*
Entry	R	*anti* : *syn*	*anti* : *syn*	*anti* : *syn*
1	BnNH	66:34	74:26	72:18
2	MeC(O)NH	3:97	2:98	10:90
3	$CF_3C(O)NH$	25:75	22:78	25:75
4	*t*-BuOC(O)NH	18:82	19:81	20:80
5	MeO[a]	100:0	100:0	100:0

[a]*In this case only one transition state really needs to be considered.*

Comparison of the two sets of transition state energy data shows that only for BnNH (Table 3, entry 1) there is more than a single transition state of importance. For the other compounds the effects are much less significant. If these data are compared to the experimentally obtained ratios (Table 1), the calculated ratios agree well with experiment.

Finally, other groups have noted that there is a direct correlation between the strength of the hydrogen bond initiated from the chiral ligand and the stereoselectivity,[21] and therefore the partial charges have been calculated, through the Merz-Kollman scheme (Table 4). It should be noted that for BnNH the NH moieties can function both as a hydrogen-bond donor and as a hydrogen bond acceptor, making it unclear whether it can be compared directly with the other three groups studied.

Table 4 Polarity of the NH bonds in auxiliary ligands.

Entry	R	q_N	q_H	Δq
1	BnNH	-0.48	0.27	0.75
2	MeC(O)NH	-0.76	0.34	1.09
3	$CF_3C(O)NH$	-0.55	0.28	0.82
4	*t*-BuOC(O)NH	-0.78	0.36	1.14

The data shows that the partial charge on H, q_H, is not affected much by the nature or oxidation level of the attached group, whereas the partial charge on N, q_N, changes significantly, reflecting the fact that for the amides, the nitrogen is part of a conjugated system. It is also clear that the electron-withdrawing effect of the trifluoroacetamide group lowers the charge of the nitrogen atom and thereby lowers the bond polarity (Δq), i.e. the difference in the partial charges on H and N. The result should be a weaker hydrogen-bonding interaction, leading to poorer selectivity. The bond polarity for both **8** and **10** is higher than for **9**, which indeed correlates to the higher selectivity for the former two over the latter. There may be limits to using a relatively crude measure like bond polarity, given that it ignores all other effects and does not take into account experimental error bars as well. Thus, for example, experimentally acetamide **8** provides higher selectivity than the carbamate **10**, which is not reflected in a higher bond polarity.

Conclusions

In conclusion we have demonstrated that the stereoselectivity of Diels-Alder reactions of suitably constructed anthracenes may be controlled through judicious choice of the protecting group used on the nitrogen atom. We have examined these processes in depth using computational methods to develop and substantiate the key control elements in these reactions that may pave the way in helping to develop more sophisticated stereoselective processes.

Experimental

Materials and methods

All solvents were obtained dry from a Grubbs dry solvent system and glassware was flame dried and cooled under vacuum before use. All dry reactions were carried out under nitrogen. TLC was carried out using Merck aluminium TLC sheets (silica gel 60 F_{254}), visualisation of TLC plates was performed using a UV lamp or by dipping in $KMnO_4$ then exposure to heat. Flash column chromatography was carried out with silica gel 40-63μ 60Å (Fluorochem Limited). ^1H and ^{13}C NMR spectra were measured using $CDCl_3$ as solvent unless otherwise stated, on a Brüker 250 or 400 MHz machine with an automated sample changer (unless otherwise stated). Chemical shifts for carbon and hydrogen are given on the δ scale relative to TMS (tetramethylsilane, δ = 0 ppm). Coupling constants were measured in Hz. ^{13}C NMR spectra were recorded using the JMOD method. Specific rotations were performed on an Optical Activity Ltd. AA-10 automatic polarimeter at 589nm (Na D-Line) and measured at 20 ^oC unless otherwise stated. $[\alpha]_D$ values are given in 10^{-1} deg cm^2 g^{-1}. Infrared spectra were recorded on a Perkin-Elmer 100 FT-IR machine using attenuated total reflectance (ATR). Mass spectra were either recorded on a micromass autospec (EI^+) or Waters LCT Classic (TOF ES^+). All chemicals were used as received without further purification. The preparation of compounds **3**, **7** and **8** were carried out by literature methods and are detailed in the supplementary information.

X-ray crystallographic data collected were measured on a Bruker Smart 1000 CCD area detector with Oxford Cryosystems low temperature system held at 150K. Reflections were measured from a hemisphere of data collected of frames each covering 0.3 degrees in omega, all of which were corrected for Lorentz and polarisation effects and for absorption by semi empirical methods based on symmetry-equivalent and repeated reflections (SADABS). All structures were solved by direct methods and refined by full matrix least squares methods on F2. Hydrogen atoms were calculated and refined in riding mode. Complex scattering factors were taken from the program package SHELXTL[24] as implemented on the Viglen Pentium computer.

Synthetic procedures

***N*-Benzyl-α-methyl-9-anthracenemethanamine 5** Magnesium sulfate (0.50 g, 4.86 mmol) was added to a stirred solution of 9-anthraldehyde **4** (3.00 g, 14.6 mmol) in dry THF (60 mL).

Benzylamine (1.8 mL, 16.2 mmol) was added drop-wise at room temperature. The resulting mixture was stirred for further 2 h at room temperature, filtered through Celite and the solvent removed under vacuum to give the imine as a yellow solid with no further purification required (4.30 g, >99%); mp 86–87 °C (lit.[25] 90–91 °C); δ_H (250 MHz; $CDCl_3$; Me_4Si) 9.57 (1 H, t, *J* 1.4, C*H*=N), 8.56–8.50 (3 H, m, ArC*H*), 8.04–7.98 (2 H, m, ArC*H*), 7.55–7.28 (9 H, m, ArC*H*), 5.16 (2 H, s, PhCH_2); δ_C (62.5 MHz; $CDCl_3$; Me_4Si) 161.0 (*C*H=N), 139.1 (Ar*C*), 131.1 (Ar*C*), 130.0 (Ar*C*), 129.4 (Ar*C*H), 128.9 (Ar*C*H), 128.7 (Ar*C*H), 128.6 (Ar*C*H), 128.3 (Ar*C*H), 128.1 (Ar*C*H), 127.0 (Ar*C*H), 126.6 (Ar*C*H), 125.5 (Ar*C*H), 125.1 (Ar*C*H), 124.7 (Ar*C*H), 66.7 (Ph*C*H_2). NMR data was in broad accordance with the literature. The complexity of the ^{13}C NMR region precludes accurate assignment.

This product (1.00 g, 3.40 mmol) was immediately dissolved in dry toluene (40 mL) and cooled to -20 °C and $BF_3.OEt_2$ (1.0 mL, 6.80 mmol) was added. The reaction mixture was stirred for 5 min at -20 °C, cooled to -78 °C and MeLi (1.6 M in Et_2O, 17.6 mL, 27.2 mmol) was added drop-wise. The resulting mixture was stirred for 6 h, allowed to warm to room temperature and stirred for further 12 h. The reaction was quenched with saturated $NaHCO_{3(aq)}$ (30 mL), the organic layer was separated, the aqueous layer was extracted with EtOAc (3 × 15 mL). The organic phases were combined, washed with brine (2 × 30 mL), and dried over Na_2SO_4. Filtration and evaporation of the solvent *in vacuo* gave the crude material that was purified by chromatography on silica gel (5% EtOAc / petroleum ether 40–60 °C) to give the title compound **5** as dark brown oil (0.45 g, 40%); ν_{max} /cm^{-1} 2920, 2905, 2860, 1662, 1600; δ_H (250 MHz; $CDCl_3$; Me_4Si) 8.40 (1 H, s, ArC*H*), 8.04–7.99 (2 H, m, ArC*H*), 7.55–7.40 (4 H, m, ArC*H*), 7.38–7.19 (7 H, m, ArC*H*), 5.54 (1 H, q, *J* 6.9, CH_3CH), 3.75 (1 H, d, *J* 12.4, PhC*H*H), 3.62 (1 H, d, *J* 12.4, PhC*H*H), 1.90 (1 H, br s, N*H*), 1.81 (3 H, d, *J* 6.9, CH_3); δ_C (62.5 MHz; $CDCl_3$; Me_4Si) 140.9 (Ar*C*), 135.7 (Ar*C*), 129.9 (Ar*C*), 129.3 (Ar*C*H), 128.3 (Ar*C*H), 128.2 (Ar*C*H), 127.5 (Ar*C*H), 126.8 (Ar*C*H), 124.7 (Ar*C*H), 52.9 (*C*H), 52.6 (CH_2), 22.3 (CH_3); *m/z* (TOF ES^+) 312.1748 (15%, MH^+. $C_{23}H_{22}N$ requires 312.1752), 205 (100).

(±)-*N*-(1-Anthracen-9-yl-ethyl)-trifluoroacetamide 9

Trifluoroacetic anhydride (1.3 mL, 9.3 mmol) was added drop-wise to a solution of 9-anthrylethanamine **3** (1.04 g, 4.69 mmol) in CH_2Cl_2 (20 mL) and left to stir under a nitrogen atmosphere at room temperature for 24 h. The solvent was evaporated and the solid obtained purified by column chromatography on silica gel, eluting with 10% EtOAc / petroleum ether 40-60 to yield the title compound **9** as yellow crystals (1.31g, 88%). A sample was crystallized from toluene for characterization purposes. mp 162–163 °C; (Found: C, 67.75; H, 4.48; N, 4.31. $C_{18}H_{14}F_3NO$ requires: C, 68.13; H, 4.45; N, 4.41); ν_{max} /cm^{-1} 3431, 3054, 1724; δ_H (400 MHz; $CDCl_3$; Me_4Si) 8.43 (1 H, s, ArC*H*), 8.27 (2 H, d, *J* 9.2, ArC*H*), 8.01 (2 H, d, *J* 8.0, ArC*H*), 7.57–7.41 (4 H, m, ArC*H*), 7.25 (1 H, br s, N*H*), 6.54 (1 H, quin, *J* 6.9, C*H*N), 1.97 (3 H, d, *J* 6.9, CH_3); δ_C (100 MHz; $CDCl_3$; Me_4Si) 156.8 (q, $J_{C\text{-}F}$ 37.1, *C*OCF_3), 131.7 (Ar*C*), 131.1 (Ar*C*), 130.1 (Ar*C*H), 129.0 (Ar*C*H), 128.8 (Ar*C*), 127.0 (2 × Ar*C*H), 125.1 (2 × Ar*C*H), 123.0 (2 × Ar*C*H), 115.8 (q, $J_{C\text{-}F}$ 288.0, *C*F_3), 46.1 (*C*HNH), 21.0 (*C*H_3); *m/z* (TOF ES^+) 360 (10%), 356 (30), 340 (60, MNa^+), 355 (100), 318.1095 (52%, MH^+. $C_{18}H_{15}F_3NO$ requires 318.1106), 205 (85).

(±)-(1-Anthracen-9-yl-ethyl)-carbamic acid *tert*-butyl ester 10

Sodium hydrogen carbonate (3.10 g, 22.4 mmol) and di-*tert*-butyl dicarbonate (2.41 g, 11.0 mmol) were added to a stirred solution of 9-anthrylethylamine **3** (1.58 g, 7.14 mmol) in EtOH (50 mL). After 72 h at room temperature, the suspension was concentrated under reduced pressure, redissolved in diethyl ether (100 mL) and filtered through a Celite® plug. The filtrate was dried over sodium sulfate, filtered and evaporated. The solid was purified by flash chromatography on silica gel eluting with 10% EtOAc / petroleum ether 40-60 to yield the title compound **10** as orange yellow crystals (1.29 g, 56%). A sample was crystallised from toluene for characterization purposes. Mp (toluene) 148–149 °C; (Found: C, 78.23; H, 7.39; N, 4.29. $C_{21}H_{23}NO_2$ requires C, 78.47; H, 7.21; N, 4.36); ν_{max}/cm^{-1} 3686, 3447, 3054, 2985, 1708; δ_H (400 MHz; $CDCl_3$; Me_4Si) 8.45 (2 H, d, *J* 9.1, ArC*H*), 8.41 (1 H, s, ArC*H*), 8.02 (2 H, d, *J* 8.2, ArC*H*), 7.45–7.60 (4 H, m, ArC*H*), 6.36 (1 H, br s, *C*HCH_3), 5.53 (1 H, br s, N*H*), 1.94 (3 H, d, *J* 6.9, CHCH_3), 1.42 [9 H, s, C(CH_3)$_3$]; δ_C (100 MHz; $CDCl_3$; Me_4Si) 155.5 (NH*C*O), 134.5 (Ar*C*), 131.8 (2 × Ar*C*), 129.7 (2 × Ar*C*H), 128.7 (2 × Ar*C*), 127.9 (Ar*C*H), 126.0 (2 × Ar*C*H), 124.8 (2 × Ar*C*H), 124.2 (2 × Ar*C*H), 79.6 [O*C*(CH_3)$_3$], 46.0 (*C*HNH), 28.4 [C(CH_3)$_3$], 22.1 (CH*C*H_3); *m/z* (TOF ES^+) 344.1633 (90%, MNa^+ requires 344.1626), 205 (100).

(±)-(3a*R*,9a*R*)-*rel*-3a,4,9,9a-tetrahydro-4-[(1*R*)-1-*N*-benzylaminoethyl]-2-methyl-,4,9[1',2']-benzeno-1*H*-benz[*f*]isoindole-1,3(2*H*)-dione 11

Benzylamine **5** (0.30 g, 0.97 mmol) was dissolved in dry toluene (10 mL) and the resulting solution was heated to 80–85 °C. *N*-Methylmaleimide (0.11 g, 1.00 mmol) was added as a solid and the reaction mixture was stirred for 4 h at 80–85 °C. The reaction mixture was allowed to cool to room temperature, and the solvent was removed under reduced pressure to afford the title cycloaddition adduct as two diastereoisomers in ratio of 73:27 in favour of the *anti*-isomer. The crude material was dissolved in toluene (8 mL) and diethyl ether (10 mL) was added slowly at room temperature. After standing, the major diastereoisomer precipitated as a white solid (0.25 g, 61% yield). The major isomer *anti* **11** was further purified for analytical purposes by diffusion recrystallisation using CH_2Cl_2 / petroleum ether 40–60, mp 200–202 °C; ν_{max} /cm^{-1} 2950, 2873, 1769, 1695; 1453, 1429; δ_H (250 MHz; $CDCl_3$; Me_4Si) 7.76–7.71 (1 H, m, ArC*H*), 7.49 (2 H, d, *J* 7.0, ArC*H*), 7.42–7.23 (6 H, m, ArC*H*), 7.22–7.11 (4 H, m, ArC*H*), 4.71 (1 H, d, *J* 3.3, C*H*), 4.61 (1 H, q, *J* 6.7, CH_3CH), 4.30 (1 H, d, *J* 17.6, PhC*H*H), 4.15 (1 H, d, *J* 17.6, PhC*H*H), 3.89 (1 H, d, *J* 8.3, C*H*), 3.15 (1 H, dd, *J* 8.3, 3.3, C*H*), 2.47 (3 H, s, NCH_3), 1.84 (3 H, d, *J* 6.7, CH_3), 1.66 (1 H, br s, N*H*); δ_C (62.5 MHz; $CDCl_3$; Me_4Si) 177.0 (*C*O), 176.2 (*C*O), 143.0 (Ar*C*), 141.4 (Ar*C*), 140.0 (Ar*C*), 139.5 (Ar*C*), 139.0 (Ar*C*), 128.4 (4 × Ar*C*H), 127.0 (Ar*C*H), 126.7 (Ar*C*H), 126.6 (Ar*C*H), 126.4 (Ar*C*H), 126.0 (Ar*C*H), 125.8 (Ar*C*H), 125.1 (Ar*C*H), 124.4 (Ar*C*H), 123.9 (Ar*C*H), 118.9 (Ar*C*H), 55.2 (*C*), 53.2 (Ph*C*H_2), 51.4 (CH_3CH), 48.8 (*C*H), 47.1 (*C*HCO), 46.5 (*C*HCO), 24.1 (NCH_3), 19.2 (CH_3); *m/z* (TOF ES^+) 423.2081 (100%, MH^+. $C_{28}H_{27}N_2O_2$ requires 423.2073). Selected

^{1}H NMR signals for the minor diastereoisomer *syn* **11**, δ_H (250 MHz; $CDCl_3$; Me_4Si) 3.86 (1H, d, *J* 3.3, C*H*), 3.22 (1H, dd, *J* 8.4, 3.3, C*H*), 1.86 (3H, d, *J* 3.1, CH_3).

(±)-(3a*S*,9a*S*)-3a,4,9,9a-Tetrahydro-4-[(1*R*)-ethylacetamido]-2-methyl-4,9-[1',2']benzeno-1*H*-benzo[*f*]isoindole-1,3-(2*H*)-dione 12 *rac-N*-[1-(9-anthryl)ethyl]acetamide **8** (0.26 g, 0.97 mmol) was dissolved in dry toluene (10 mL) and the resulting solution was heated to 80–85 °C. *N*-Methylmaleimide (0.11 g, 1.00 mmol) was added as a solid and the reaction mixture was stirred for 4 h at 80–85 °C The reaction mixture was allowed to cool to room temperature, and the solvent was removed under reduced pressure to afford the title cycloaddition adduct as two diastereoisomers in ratio of 90:10 in favour of the *syn*-isomer. The crude material was recrystallised from CH_2Cl_2/hexane to afford a single diastereoisomer of the title compound *syn* **12** as a white powder (0.20 g, 55% yield); mp 299–303 °C; ν_{max} /cm^{-1} 3505, 3050, 1693, 1669; δ_H (250 MHz; $CDCl_3$; Me_4Si) 7.63–7.57 (1 H, m, ArC*H*), 7.44–7.41 (1 H, m, ArC*H*), 7.27–7.15 (3 H, m, ArC*H*), 7.13–7.05 (3 H, m, ArC*H*), 6.12 (1 H, d, *J* 7.3, N*H*), 5.60 (1 H, quint, *J* 6.7, CH_3C*H*), 4.69 (1 H, d, *J* 2.4, C*H*), 3.27–3.05 (2 H, m, 2 × C*H*), 2.40 (3 H, s, NCH_3), 1.91 (3 H, s, COCH_3), 1.89 (3 H, d, *J* 6.7, CH_3); δ_C (63 MHz; $CDCl_3$; Me_4Si) 176.2 (*C*O), 174.5 (*C*O), 169.5 (*C*O), 143.5 (Ar*C*), 138.8 (Ar*C*), 138.5 (Ar*C*), 127.5 (Ar*C*H), 127.2 (Ar*C*H), 127.1 (Ar*C*H), 126.5 (Ar*C*H), 125.5 (Ar*C*H), 125.0 (Ar*C*H), 124.0 (Ar*C*H), 123.5 (Ar*C*H), 118.9 (Ar*C*), 52.1 (*C*), 48.5 (*C*H), 47.0 (*C*H), 45.9 (*C*H), 44.9 (*C*H), 24.3 (*C*H$_3$), 23.7 (*C*H$_3$), 17.1 (*C*H$_3$); *m/z* (EI$^+$) 374.1627 (4%, M$^+$. $C_{23}H_{22}N_2O_3$ requires 374.1630), 331 (10), 264 (37), 263 (100), 220 (59), 206 (45), 179 (30), 112 (12). Selected ^{1}H NMR signals for the minor diastereoisomer *anti* **12**, δ_H (250 MHz; $CDCl_3$; Me_4Si) 4.59 (1H, d, *J* 3.1, C*H*), 2.29 (3H, s, NCH_3), 1.74 (3H, s, COCH_3), 1.68 (3H, d, *J* 6.4, CH_3).

(±)-(3a*S*,9a*S*)-3a,4,9,9a-Tetrahydro-4-[(1*R*)-ethyl-trifluoroacetamido]-2-methyl-4,9-[1',2']benzeno-1*H*-benzo[*f*]isoindole-1,3-(2*H*)-dione 13 *rac-N*-[1-(9-Anthryl)ethyl]trifluoroacetamide **9** (0.31 g, 0.97 mmol) was dissolved in dry toluene (10 mL) and the resulting solution was heated to 80–85 °C. *N*-Methylmaleimide (0.11 g, 1.00 mmol) was added as a solid and the reaction mixture was stirred for 4 h at 80–85 °C The reaction mixture was allowed to cool to room temperature, and the solvent was removed under reduced pressure to afford the title cycloaddition adduct as two diastereoisomers in ratio of 75:25 in favour of the *syn*-isomer. The crude material was recrystallised from CH_2Cl_2/hexane to afford a single diastereoisomer of the title compound *syn* **13** as white crystals (0.25 g, 60% yield); mp 250–251 °C; ν_{max} /cm^{-1} 3684, 3433, 3024, 1776, 1725, 1701; δ_H (250 MHz; $CDCl_3$; Me_4Si) 7.61–7.48 (2 H, m, ArC*H*), 7.33–7.24 (3 H, m, ArC*H*), 7.20–7.16 (2 H, m, ArC*H*), 7.11–7.03 (1 H, m, ArC*H*), 6.96 (1 H, d, *J* 6.9, N*H*), 5.72 (1 H, quin, *J* 6.9, NHC*H*), 4.78 (1 H, d, *J* 2.9, C*H*), 3.31–3.22 (2 H, m, 2 × C*H*), 2.48 (3 H, s, CH_3N), 2.03 (3 H, d, *J* 6.9, CHCH_3); δ_C (125 MHz; $CDCl_3$; Me_4Si) 175.9 (N*C*O), 174.5 (N*C*O), 156.7 (q, $J_{C\text{-}F}$ 37, *C*OCF$_3$), 143.4 (Ar*C*), 138.5 (Ar*C*), 137.8 (Ar*C*), 137.6 (Ar*C*), 127.6 (2 × Ar*C*H), 127.5 (Ar*C*H), 126.9 (Ar*C*H), 125.9 (Ar*C*H), 125.4 (Ar*C*H), 123.1 (Ar*C*H), 122.7 (Ar*C*H), 115.7 (q, $J_{C\text{-}F}$ 288, *C*F$_3$), 51.6 (*C*), 48.3 (*C*H), 46.9 (*C*H), 46.1 (*C*H), 45.8 (*C*H), 24.4 (NCH_3), 16.4 (CH*C*H$_3$); *m/z* (TOF ES$^+$) 451 (100%, MNa$^+$), 429.1429 (74, MH$^+$. $C_{23}H_{20}F_3N_2O_3$ requires 429.1426). Selected ^{1}H NMR signals for the minor diastereoisomer *anti* **13**, δ_H (250 MHz; $CDCl_3$; Me_4Si) 4.67 (1 H, d, *J* 2.8, C*H*), 3.57 (1 H, d, *J* 8.5, COC*H*), 3.40 (1 H, dd, *J* 8.5, 2.8, COC*H*), 2.71 (3 H, s, CH_3N), 1.83 (3 H, d, *J* 6.9, CH_3).

(±)-(3a*S*,9a*S*)-3a,4,9,9a-Tetrahydro-4-[(1*R*)-ethyl-*tert*-butylcarbamato]-2-methyl-4,9-[1',2']benzeno-1*H*-benzo[*f*]isoindole-1,3-(2*H*)-dione 14 *rac-N*-[1-(9-Anthryl)ethyl]-carbamic acid *tert*-butyl ester **10** (0.31 g, 0.97 mmol) was dissolved in dry toluene (10 mL) and the resulting solution was heated to 80–85 °C. *N*-Methylmaleimide (0.11 g, 1.00 mmol) was added as a solid and the reaction mixture was stirred for 4 h at 80–85 °C The reaction mixture was allowed to cool to room temperature, and the solvent was removed under reduced pressure to afford the title cycloaddition adduct as two diastereoisomers in a ratio of 80:20 in favour of the *syn*-isomer. The crude material was recrystallised from CH_2Cl_2/hexane to afford a single diastereoisomer of the title compound *syn* **14** as white crystals (0.23 g, 54% yield); mp 235–236 °C; ν_{max} /cm^{-1} 3684, 3027, 1775, 1700; δ_H (500 MHz; $CDCl_3$; Me_4Si) 7.66 (1 H, d, *J* 6.8, ArC*H*); 7.45 (1 H, dd, *J* 7.2, 2.1, ArC*H*), 7.31-7.20 (4 H, m, ArC*H*), 7.09–7.06 (2 H, m, ArC*H*), 5.48-5.38 (1 H, br m, NC*H*CH$_3$), 5.31-5.23 (1 H, br m, NH), 4.73 (1 H, s, C*H*), 3.22 (2 H, s, 2 × C*H*), 2.46 (3 H, s, NCH_3), 1.94 (3 H, d, *J* 6.8, NCHCH_3), 1.45 [9 H, br s, (CH_3)$_3$C]; δ_C (125 MHz; $CDCl_3$; Me_4Si) 176.3 (MeN*C*=O), 174.6 (MeN*C*=O), 155.4 (^{t}BuO*C*=O), 143.3 (Ar*C*), 138.8 (Ar*C*), 138.7 (Ar*C*), 138.5 (Ar*C*), 127.3 (Ar*C*H), 127.1 (Ar*C*H), 126.9 (Ar*C*H), 126.4 (Ar*C*H), 125.2 (Ar*C*H), 124.9 (Ar*C*H), 124.4 (Ar*C*H), 123.8 (Ar*C*H), 79.5 (O*C*), 52.5 (*C*), 48.5 (*C*H), 47.1 (*C*H), 45.9 (*C*H), 28.4 [(*C*H$_3$)$_3$], 24.2 (NCH_3), 17.7 (CH*C*H$_3$); *m/z* (TOF ES$^+$) 455 (30%, MNa$^+$), 450 (100), 433.2137 (10, MH$^+$. $C_{26}H_{29}N_2O_4$ requires 433.2127), 377 (22), 333 (20). Selected ^{1}H NMR signals for the minor diastereoisomer, as a mixture of rotamers, δ_H (250 MHz; $CDCl_3$; Me_4Si) 4.64 (1 H, d, *J* 3.1, C*H*), 3.46 (1 H, d, *J* 8.9, C*H*), 3.13 (1 H, dd, *J* 8.2, 3.1, C*H*), 1.86 (3 H, d, *J* 6.4, CH_3 rotamer A), 1.73 (3 H, d, *J* 6.4, CH_3, rotamer B).

Crystallography

Crystal data for **11** (coded as OSJ27) $C_{28}H_{26}N_2O_2$; M = 422.51; crystallises from dichloromethane/petroleum ether as colourless plates; crystal dimensions 0.43 x 0.32 x 0.32 mm^3. Triclinic, a = 10.2636(18), b = 10.7862(18), c = 11.475(2) Å, α= 96.250(3)°, β= 98.454(3)° γ = 104.549(3)°, *U* = 1202.0(4) Å^3, Z = 2, Dc = 1.167 Mg/m^3, space group P-1 (C1i , No. 2) , Mo-Kα radiation ($\bar{\lambda}$ = 0.71073 Å), μ (Mo-Kα) = 0.0741 mm^{-1}, F(000) = 448. Final R = 0.0539 (wR$_2$ = 0.1683, for all 4236 data, 294 parameters, mean and maximum δ/σ 0.000,0.000) with allowance for the thermal anisotropy of all non-hydrogen atoms. Minimum and maximum final electron density -0.556 and 0.668 e.Å^{-3}. A weighting scheme w = 1/[σ^2 (Fo^2) +(0.0954*P)^2+0.4985*P] where P=(Fo^2+ 2 * Fc2)/3 was used in the latter stages of refinement

Crystal data for **12** (coded as osj19) $C_{23}H_{22}N_2O_3$; M = 374.43. Crystallises from dichloromethane/petroleum ether as colourless block; crystal dimensions 0.41 x 0.32 x 0.23 mm. Orthorhombic, *a* = 17.583(2), *b* = 11.5915(14), *c* = 17.893(2) Å, *U* = 3646.9(8) Å^3, *Z* = 8, *D*c = 1.364 Mg/m^3, space group Pbca

(D_2^{15}, No.61), Mo-Kα radiation ($\bar{\lambda}$ = 0.71073 Å), μ(Mo-Kα) = 0.091 mm^{-1}, F(000) = 1584. Data collected were measured on a Bruker Smart CCD area detector with Oxford Cryosystems low temperature system. Cell parameters were refined from the setting angles of 3981 reflections (θ range 2.28 < 25.00°). Final R = 0.0506 (wR_2 = 0.1470, for all 3215 data, 256 parameters, mean and maximum δ/σ 0.000,0.000) with allowance for the thermal anisotropy of all non-hydrogen atoms. Minimum and maximum final electron density -0.237 and 0.755e. $Å^{-3}$. A molecule of acetonitrile was found to be present. A weighting scheme $w = 1/[\sigma^2(Fo^2) + (0.0549*P)^2 + 4.0964*P]$ where $P=(Fo^2 + 2 * Fc^2)/3$ was used in the latter stages of refinement.

Crystal data for **13** (coded as OSJ51) $C_{23}H_{19}F_3N_2O_3$; M = 425. Crystallises from chloroform and 40/60 petroleum ether as pale yellow needles; crystal dimensions 0.30 x 0.06 x 0.06 mm^3. Orthorhombic, a = 14.680(3), b = 17.220(3), c = 15.260(3) Å, *U* = 3857.6(13) $Å^3$, Z = 8, Dc = 1.475 Mg/m^3, space group Pbca (D_2^{15}, No.61), Mo-Kα radiation ($\bar{\lambda}$ = 0.71073 Å), μ (Mo Kα) = 2.208 mm^{-1}, F(000) = 1776. Final R = 0.0458 (wR_2 = 0.1299, for all 2977 data, 281 parameters with allowance for the thermal anisotropy of all non-hydrogen atoms. Minimum and maximum final electron density -0.289 and 0.277e. $Å^{-3}$. A weighting scheme $w = 1/[\sigma^2 (Fo^2) + (0.0326*P)^2 + 0.00*P]$ where $P=(Fo^2 + 2 * Fc^2)/3$ was used in the latter stages of refinement.

Crystal data for **14** (coded as OSJ53) $C_{26}H_{28}N_2O_4$; M = 432.50, crystallises from dichloromethane as colourless blocks; crystal dimensions 0.32 x 0.14 x 0.06 mm^3. Monoclinic, *a* = 14.9540(12), *b* = 9.4917(8), *c* = 16.5072(6) Å, β = 107.913(3)° *U* = 2229.4(3) $Å^3$, *Z* = 4, *D*c = 1.289 Mg/m^3, space group $P2_1/c$ (C_2^5 *h,* No.14), Mo-Kα radiation ($\bar{\lambda}$ = 0.71073 Å), μ(Mo-Kα) = 0.087 mm^{-1}, F(000) = 920. Final R = 0.0517 (wR_2 = 0.1555, for all 3916 data, 294 parameters, mean and maximum δ/σ 0.000,0.000) with allowance for the thermal anisotropy of all non-hydrogen atoms. Minimum and maximum final electron density -0.284 and 0.242 e.$Å^{-3}$. A weighting scheme $w = 1/[\sigma^2(Fo^2) + (0.0729*P)^2 + 0.2665*P]$ where $P = (Fo^2 + 2 * Fc^2)/3$ was used in the latter stages of refinement.

Computational

All of the calculations were performed using density functional theory (DFT) with the B3LYP hybrid functional[26–29] using the 6-311G(d,p) basis set[30] for all atoms as implemented in Gaussian 09.[31] Solvent effects were included in all of the calculations through the IEF-PCM[32] model as implemented in Gaussian 09[31] with toluene as the solvent. These computational parameters were chosen to allow comparison with previous work.[18] Moreover, B3LYP has been found to determine stereoselectivities accurately and has been used in the past in the study of Diels-Alder reactions.[18,20,21,33]
All of the reactant, transition state, and product structures were fully optimized without any symmetry restrictions. Transition states were located using the QST3 algorithm.[34] Frequency calculations were carried out to characterize all stationary points obtained to confirm them as either local minima or transition states. Frequencies were used to calculate free energies in the standard way. The free energy of activation used is defined as the difference in free energy between the transition state and infinitely separated reactants. It is noted that the formation of a pre-collision complex was found to be endergonic in all cases. Transition states were identified by their single imaginary frequency. A visual inspection was carried out for each of the transition states to confirm it connected the correct reactants and products.

Acknowledgements

We thank the Committee of Higher Education in Libya and the Libyan Arab Peoples Bureau for a scholarship (RAB) and the University of Sheffield (FMG) for funding. Calculations were performed on the 'Sol' cluster of the Theoretical Chemistry Group at the University of Sheffield (UoS) and on the central 'Iceberg' cluster of the UoS.

Notes and references

1. M. J. Fisher, W. J. Hehre, S. D. Kahn, and L. E. Overman, *J. Am. Chem. Soc.*, 1988, **110**, 4625–4633.

2. S. C. Datta, R. W. Franck, R. Tripathy, G. J. Quigley, L. Huang, S. Chen, and A. Sihaed, *J. Am. Chem. Soc.*, 1990, **112**, 8472–8478.

3. B. M. Trost and D. C. Lee, *J. Org. Chem.*, 1989, **54**, 2271–2274.

4. H. Jiang, C. Rodríguez-Escrich, T. K. Johansen, R. L. Davis, and K. A. Jørgensen, *Angew. Chem. Int. Ed. Engl.*, 2012, **51**, 10271–4.

5. T. R. Kelly, P. Meghani, and V. S. Ekkundi, *Tetrahedron Lett.*, 1990, **31**, 3381–3384.

6. M. Shoji, H. Imai, I. Shiina, H. Kakeya, H. Osada, and Y. Hayashi, *J. Org. Chem.*, 2004, **69**, 1548–56.

7. J. C. Christian Atherton and S. Jones, *J. Chem. Soc. Perkin Trans. 1*, 2002, 2166–2173.

8. H. Adams, S. Jones, A. J. H. M. Meijer, Z. Najah, I. Ojea-Jimenez, and A. T. Reeder, *Tetrahedron Asymmetry*, 2011, **22**, 1620–1625.

9. S. A. Hasbullah and S. Jones, *Tetrahedron: Asymmetry*, 2010, **21**, 2719–2725.

10. J. C. Ball, R. Gleave, and S. Jones, *Org. Biomol. Chem.*, 2011, **9**, 4353–4360.

11. H. Adams, S. Jones, and I. Ojea-Jimenez, *Org. Biomol. Chem.*, 2006, **4**, 2296–2303.

12. K. L. Burgess, N. J. Lajkiewicz, A. Sanyal, W. Yan, and J. K. Snyder, *Org. Lett.*, 2005, **7**, 31–34.

13. M. S. Corbett, X. Liu, A. Sanyal, and J. K. Snyder, *Tetrahedron Lett.*, 2003, **44**, 931–935.

14. A. Sanyal and J. K. Snyder, *Org. Lett.*, 2000, **2**, 2527–2530.

15. X. Liu and J. K. Snyder, *J. Org. Chem.*, 2008, **73**, 2935–2938.

16. A. L. Jones, X. Liu, and J. K. Snyder, *Tetrahedron Lett.*, 2010, **51**, 1091–1094.

17. K. L. Burgess, M. S. Corbett, P. Eugenio, N. J. Lajkiewicz, X. Liu, A. Sanyal, W. Yan, Q. Yuan, and J. K. Snyder, *Bioorg. Med. Chem.*, 2005, **13**, 5299–5309.

18. H. Adams, T. M. Elsunaki, I. Ojea-Jiménez, S. Jones, and A. J. H. M. Meijer, *J. Org. Chem.*, 2010, **75**, 6252–6262.

19. J. C. C. Atherton and S. Jones, *Tetrahedron Lett.*, 2001, **42**, 8239–8241.

20. N. Celebi-Olçüm, A. Sanyal, and V. Aviyente, *J. Org. Chem.*, 2009, **74**, 2328–36.

21. S. Agopcan, N. Çelebi-Ölçüm, M. N. Üçışık, A. Sanyal, and V. Aviyente, *Org. Biomol. Chem.*, 2011, **9**, 8079–88.

22. H. Adams, R. A. Bawa, K. G. McMillan, and S. Jones, *Tetrahedron: Asymmetry*, 2007, **18**, 1003–1012.

23. A. Sanyal, Q. Yuan, and J. K. Snyder, *Tetrahedron Lett.*, 2005, **46**, 2475–2478.

24. *SHELXTL version, An integrated system for From, solving and refining crystal structures diffraction data (Revision 5.1), Bruker AXS LTD*, .

25. N. Giuseppone, J.-L. Schmitt, E. Schwartz, and J.-M. Lehn, *J. Am. Chem. Soc.*, 2005, **127**, 5528–39.

26. A. D. Becke, *J. Chem. Phys.*, 1993, **98**, 5648.

27. S. H. Vosko, L. Wilk, and M. Nusair, *Can. J. Phys.*, 1980, **58**, 1200–1211.

28. C. Lee, W. Yang, and R. G. Parr, *Phys. Rev. B*, 1988, **37**, 785–789.

29. B. Miehlich, A. Savin, H. Stoll, and H. Preuss, *Chem. Phys. Lett.*, 1989, **157**, 200–206.

30. R. Krishnan, J. S. Binkley, R. Seeger, and J. A. Pople, *J. Chem. Phys.*, 1980, **72**, 650.

31. M. J. Frisch, G. W. Trucks, H. B. Schlegel, G. E. Scuseria, M. A. Robb, J. R. Cheeseman, G. Scalmani, V. Barone, B. Mennucci, G. A. Petersson, H. Nakatsuji, M. Caricato, X. Li, H. P. Hratchian, A. F. Izmaylov, J. Bloino, G. Zheng, J. L. Sonnenberg, M. Hada, M. Ehara, K. Toyota, R. Fukuda, J. Hasegawa, M. Ishida, T. Nakajima, Y. Honda, O. Kitao, H. Nakai, T. Vreven, J. A. MontgomeryJr., J. E. Peralta, F. Ogliaro, M. Bearpark, J. J. Heyd, E. Brothers, K. N. Kudin, V. N. Staroverov, R. Kobayashi, J. Norman, K. Raghavachari, A. Rendell, J. C. Burant, S. S. Iyengar, J. Tomasi, M. Cossi, N. Rega, J. M. Millam, M. Klene, J. E. Knox, J. B. Cro, and D. J. Fox, 2009, Gaussian, Inc., Wallingford CT.

32. J. Tomasi, B. Mennucci, and R. Cammi, *Chem. Rev.*, 2005, **105**, 2999–3093.

33. D. F. P. Crépin, J. P. A. Harrity, J. Jiang, A. J. H. M. Meijer, A.-C. M. A. Nassoy, and P. Raubo, *J. Am. Chem. Soc.*, 2014, **136**, 8642–53.

34. C. Peng, P. Y. Ayala, H. B. Schlegel, and M. J. Frisch, *J. Comput. Chem.*, 1996, **17**, 49–56.